Nanoscale

PAPER

View Article Online
View Journal | View Issue

Cite this: *Nanoscale*, 2021, **13**, 3868

B_{48}^-: a bilayer boron cluster†

Wei-Jia Chen,‡[a] Yuan-Yuan Ma,‡[b,c] Teng-Teng Chen,[a] Mei-Zhen Ao,[b,c] Dao-Fu Yuan,[a] Qiang Chen,*[b] Xin-Xin Tian,[b] Yue-Wen Mu,[b] Si-Dian Li*[b] and Lai-Sheng Wang*[a]

Received 31st December 2020,
Accepted 7th February 2021

DOI: 10.1039/d0nr09214b

rsc.li/nanoscale

Size-selected negatively-charged boron clusters (B_n^-) have been found to be planar or quasi-planar in a wide size range. Even though cage structures emerged as the global minimum at B_{39}^-, the global minimum of B_{40}^- was in fact planar. Only in the neutral form did the B_{40} borospherene become the global minimum. How the structures of larger boron clusters evolve is of immense interest. Here we report the observation of a bilayer B_{48}^- cluster using photoelectron spectroscopy and first-principles calculations. The photoelectron spectra of B_{48}^- exhibit two well-resolved features at low binding energies, which are used as electronic signatures to compare with theoretical calculations. Global minimum searches and theoretical calculations indicate that both the B_{48}^- anion and the B_{48} neutral possess a bilayer-type structure with D_{2h} symmetry. The simulated spectrum of the D_{2h} B_{48}^- agrees well with the experimental spectral features, confirming the bilayer global minimum structure. The bilayer $B_{48}^{-/0}$ clusters are found to be highly stable with strong interlayer covalent bonding, revealing a new structural type for size-selected boron clusters. The current study shows the structural diversity of boron nanoclusters and provides experimental evidence for the viability of bilayer borophenes.

1. Introduction

To compensate for its electron deficiency, boron forms a wide variety of bulk allotropes and polyhedral boranes with different aggregation and three-dimensional (3D) structures.[1–3] In contrast to bulk boron, joint experimental and theoretical investigations have revealed that size-selected boron clusters possess two-dimensional (2D) structures for a broad size range.[4–14] Planar boron clusters consisting of B_3 triangles with tetragonal, pentagonal or hexagonal holes are characterized by localized peripheral two-center two-electron (2c–2e) B–B σ bonds and delocalized interior (*nc*–2e) σ and π bonds.[15,16] The discovery of the planar B_{36} cluster with C_{6v} symmetry and a central hexagonal hole provided the first experimental evidence for the viability of monolayer boron similar to graphene, named borophene.[17] Subsequent bonding analysis showed that the π bonding in B_{36} was analogous to that in coronene.[18] The B_{35}^- cluster was also found to be planar, but with a double hexagonal vacancy (DHV), providing a more flexible structural motif to build borophenes.[19] Borophenes have been successfully synthesized on Ag(111) substrates by two research teams,[20,21] becoming a new class of synthetic 2D materials with novel properties.[22–25] The recently reported quasi-planar B_{41}^- and B_{42}^- clusters with a DHV are the largest B_n^- clusters, whose structures have been solved using photoelectron spectroscopy (PES) and theoretical calculations.[26]

Another major breakthrough in the investigation of boron clusters is the discovery of borospherene, the fullerene-like D_{2d} B_{40} cage, which is composed of 48 B_3 triangles, two hexagons, and four heptagons.[27] However, while the borospherene cage is the global minimum for neutral B_{40}, the global minimum of the B_{40}^- anion was found to be a 2D structure with a DHV. The chiral B_{39}^- borospherene was the only negatively-charged boron cluster found to have a cage-like global minimum.[28] The seashell-like B_{28}^- and B_{29}^- were later observed as minor isomers, close in energy to their respective 2D global minima.[29–31] There was immense interest about the structural evolution of larger boron clusters beyond B_{40}^-. In particular, the question was if larger borospherenes would exist. Our recent study showed that the global minima of B_{41}^- and B_{42}^- are planar with a DHV.[26] First-principles calculations based on high-throughput screening have been used to examine the structures of larger boron clusters, revealing various 2D and tubular structures.[32,33] Sai *et al.* calculated several larger boron clusters and compared the stability of the cage structures with

[a]*Department of Chemistry, Brown University, Providence, Rhode Island 02912, USA. E-mail: lai-sheng_wang@brown.edu*
[b]*Nanocluster Laboratory, Institute of Molecular Science, Shanxi University, Taiyuan 030006, China. E-mail: chenqiang@sxu.edu.cn, lisidian@sxu.edu.cn*
[c]*Fenyang College of Shanxi Medical University, Fenyang 032200, China*

†Electronic supplementary information (ESI) available. See DOI: 10.1039/d0nr09214b

‡These authors contributed equally to this work.

that of core–shell, 2D, and bilayer structures.[34] Interestingly, they found the bilayer structure to be the global minimum for B_{48} at the TPSSh/6-311G(d) level of theory. Bilayer-type structures have also been studied recently for several larger boron clusters (B_{54}, B_{60}, and B_{62}) at the PBE0 level of theory.[35]

PES has been one of the most powerful experimental techniques to study size-selected boron clusters,[9] but it has become more challenging because photoelectron spectra become increasingly broad and featureless for larger boron clusters due to insufficient cluster cooling and/or the presence of multiple isomers. Beyond B_{42}^-, which is the largest boron cluster that has been characterized by PES,[26] the only larger B_n^- cluster displaying discernible PES features is the B_{48}^- cluster. Well-resolved PES features are critical to be used to compare with theoretical calculations. In this article, we report a combined PES and first-principles investigation on the $B_{48}^{-/0}$ clusters. Our global minimum search led to a bilayer global minimum for B_{48}^- with D_{2h} symmetry, similar to that of neutral B_{48}.[34] More importantly, the simulated spectrum of the D_{2h} B_{48}^- agrees well with the experimental data. The confirmation of the bilayer $B_{48}^{-/0}$ clusters provides experimental evidence for the viability of bilayer borophenes. The B_{48} cluster is used as a structural motif to construct different bilayer borophenes with various hole densities (η).

2. Methods

2.1 Photoelectron spectroscopy

The experiment was done using a magnetic-bottle PES apparatus equipped with a laser vaporization supersonic cluster source, details of which can be found elsewhere.[9,36] The B_{48}^- cluster was produced by laser vaporization of a hot-pressed ^{11}B-enriched disk target. Clusters formed inside the large waiting-room nozzle were entrained by a He carrier gas seeded with 5% Ar and cooled by a supersonic expansion. After passing through a skimmer, negatively-charged clusters were extracted perpendicularly from the collimated cluster beam and analyzed using a time-of-flight mass spectrometer. The B_{48}^- clusters were mass-selected and decelerated before photodetachment. Two different photon energies were used in the PES experiment, 266 nm (4.661 eV) from a Nd:YAG laser and 193 nm (6.424 eV) from an ArF excimer laser. Photoelectrons were collected at nearly 100% efficiency and analyzed in a 3.5 m long electron flight tube. The photoelectron spectra were calibrated using the known spectrum of Bi^-. The kinetic energy (E_k) resolution of the magnetic-bottle PES analyzer was about 2.5% ($\Delta E_k/E_k$), that is, ~25 meV for photoelectrons with 1 eV kinetic energy.

2.2 Computational methods

Global minimum searches for B_{48}^- and B_{48} were performed using the TGMin2 program,[37–39] in conjunction with manual structural constructions based on the known 2D, cage-like, core–shell, and tubular structures. More than 2500 trial structures were explored for each species on their respective potential energy surfaces. The resulting low-lying isomers for B_{48}^- and B_{48} were first optimized at the PBE0/6-31G(d) level, and their vibrational frequencies were checked to ensure that all isomers obtained were true minima. The thirty lowest-lying isomers of B_{48}^- were further optimized using the PBE0[40] and TPSSh[41] methods with the 6-311+G(d) basis set.[42] The relative energies of the two lowest-lying isomers were further refined by single-point coupled cluster CCSD(T)[43–45] calculations with the 6-31G(d) basis set at the PBE0/6-311+G(d) geometries. Unrestricted theoretical methods were used for systems in doublet or triplet states. The first vertical detachment energy (VDE) for B_{48}^- was calculated as the energy difference between the anionic ground state and the neutral ground state at the optimized anion geometry. Higher binding energy VDEs were calculated using the time-dependent DFT method (TD-DFT)[46,47] at the PBE0/6-311+G(d) level. All the DFT calculations in this work were performed using the Gaussian 09 program,[48] whereas the CCSD(T) calculations were done using MOLPRO 2012.[49] Bonding analyses were done using the canonical molecular orbitals (CMOs), the electron localization function (ELF),[50] and the adaptive natural density partitioning (AdNDP) method.[51,52] The AdNDP results were visualized using the VMD 1.9.3 program.[53] Born–Oppenheimer molecular dynamics (BOMD) simulations were performed on the global minima of B_{48}^- and B_{48} at 1000 K, using the CP2K software suite[54] with the GTH-PBE pseudopotential and the DZVP-MOLOPT-SR-GTH basis set. Bilayer borophenes were designed using the global minimum bilayer B_{48} clusters as structural motifs and optimized using DFT within the Perdew–Burke–Ernzerhof (PBE) exchange correlation functional of the generalized gradient approximation (GGA)[55] and projector-augmented wave (PAW) method,[56,57] as implemented in the Vienna *ab initio* simulation package (VASP) code.[58,59]

3. Results

3.1 Photoelectron spectroscopy

The photoelectron spectra of B_{48}^- at 266 nm and 193 nm are shown in Fig. 1. The 193 nm spectrum (Fig. 1b) revealed two well-resolved bands (X and A) in the low binding energy range and nearly continuous signals beyond ~4.5 eV. The bands X and A were slightly better resolved in the 266 nm spectrum (Fig. 1a), and the tail on the low binding energy side of band X was probably due to vibrational hot bands. Band X yields a ground state VDE of 3.56 eV. Since no vibrational structures were resolved for band X, the ADE was estimated by drawing a straight line along its leading edge and then adding the instrumental resolution to the intersection with the binding energy axis. The ADE so obtained was 3.3 eV, which also represents the electron affinity of neutral B_{48} and corresponds to the detachment transition from the ground state of B_{48}^- to that of neutral B_{48}. The sharper and more intense band A gave a VDE of 3.87 eV. Following an energy gap, the higher binding energy part of the 193 nm spectrum was nearly continuous, likely due to multiple detachment transitions, as expected for such a

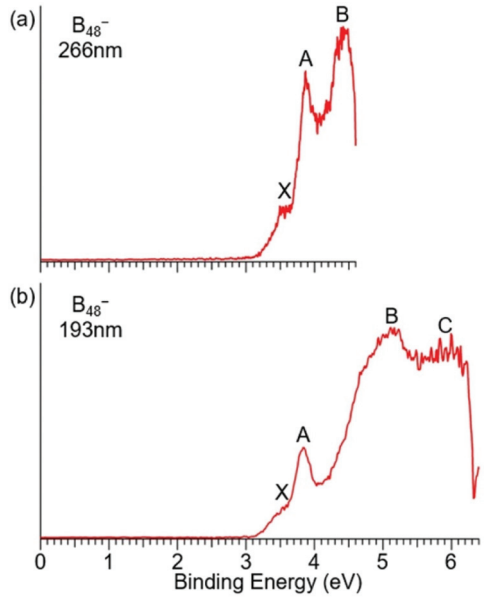

Fig. 1 The photoelectron spectra of B_{48}^- at (a) 266 nm (4.661 eV) and (b) 193 nm (6.424 eV).

large system. For the sake of discussion, we tentatively labeled the two broad spectral regions as B and C, centered around ~5.1 eV and ~5.9 eV, respectively. Despite the complexity of the photoelectron spectra, the well-resolved bands X and A followed by an energy gap provide critical spectral signatures, which can be used to compare with theoretical results.

3.2 The structures of B_{48}^- and B_{48}

The six low-lying isomers emerged from our global minimum searches are depicted in Fig. 2 for B_{48}^- (**I–VI**) and B_{48} (**VII–XII**). All isomers located within 4 eV of the global minima at the PBE0 level are given in Fig. S1 for B_{48}^- and Fig. S2 for B_{48}.†

The global minimum D_{2h} B_{48} (**VII**, ^1A_g) bilayer structure in the current work is similar to that reported previously by Sai *et al.*[34] As shown in Fig. 2(b), the bilayer D_{2h} structure lies 1.31 eV lower in energy than the second lowest-lying core–shell C_2 B_{48} (**VIII**, ^1A) at the CCSD(T) level. Sai *et al.* compared the stability of the bilayer structure with the core–shell structure **VIII** (+1.35 eV), a 2D structure with a DHV (+1.59 eV), and the borospherene structure **XII** (+1.77 eV) at the TPSSh/6-311G(d) level.[34] In a more recent study, Wu *et al.* also reported a triple-ring tubular structure which is only 0.5 eV higher in energy than the bilayer global minimum at the TPSSh/6-311+G* level.[60] In the current study, we found that the triple-ring tubular structure (**IX**) of B_{48} is 1.80 eV higher in energy than the bilayer global minimum at the CCSD(T) level. We also found two more low-lying isomers, the C_{2v} structure (**X**) at 1.45 eV and the 2D structure with a single hexagonal hole (**XI**) at 1.47 eV above the global minimum at the PBE0/6-311+G(d) level, suggesting a more complicated potential energy landscape.

The global minimum of B_{48}^- (**I**, ^2A_u) shown in Fig. 1a is similar to that of neutral B_{48}. The triple-ring tubular B_{48}^- (**II**, ^2B) was found to be closer in energy to the global minimum at the PBE0 and TPSSh levels of theory, but much higher in energy (by 1.62 eV) at the CCSD(T) level of theory. Three 2D isomers (**III**, **IV**, **V**) and the core–shell isomer **VI** were found to be more than 1 eV higher in energy at the PBE0 level and more than 0.9 eV higher in energy at the TPSSh level than the bilayer B_{48}^- global minimum. The D_{2h} bilayer structure is overwhelmingly the global minimum for both the B_{48}^- anion and the B_{48} neutral cluster at our highest level of theory. The D_{2h} symmetry of the bilayer structure makes it relatively easy to visualize it. The bilayer structure of B_{48}^- basically consists of a bilayer B_{38} hexagonal prism with two identical B_{19} layers ($B@B_6@B_{12}$) (marked by the blue dashed lines in Fig. 2), which are joined together by two V-shaped B_5 chains on the waist at the two ends. The two B_{19} layers display significant

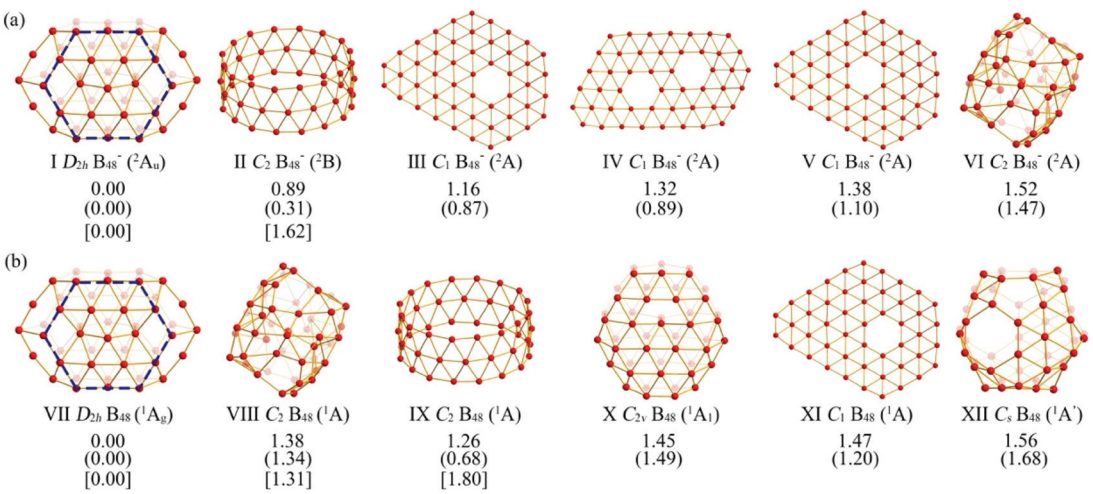

Fig. 2 The six lowest-lying isomers of B_{48}^- (a) and B_{48} (b). Relative energies are given in eV at the PBE0/6-311+G*, TPSSh/6-311+G(d) (in parentheses), and CCSD(T) (in square brackets) levels. The bilayer B_{38} hexagonal prism in **I** and **VII** are marked by the blue dashed lines.

inward buckling and form two interlayer B–B bonds in addition to the interlayer B–B bonds on the periphery. In fact, the bilayer structure can be viewed as a squashed cage-like or seashell-like structure.

4. Comparison between experiment and theory

To verify the global minimum of B_{48}^-, we computed the VDEs of the two lowest-lying isomers, the bilayer B_{48}^- (**I**) and the tubular B_{48}^- (**II**), using TD-DFT at the PBE0 level. The computed VDEs were fitted with unit-area Gaussians of 0.1 eV width to produce simulated PE spectra, as compared with the 193 nm data in Fig. 3. The computed VDEs for the bilayer D_{2h} B_{48}^- (**I**) along with the final electronic states and electron configurations are compared with the experimental data in Table 1.

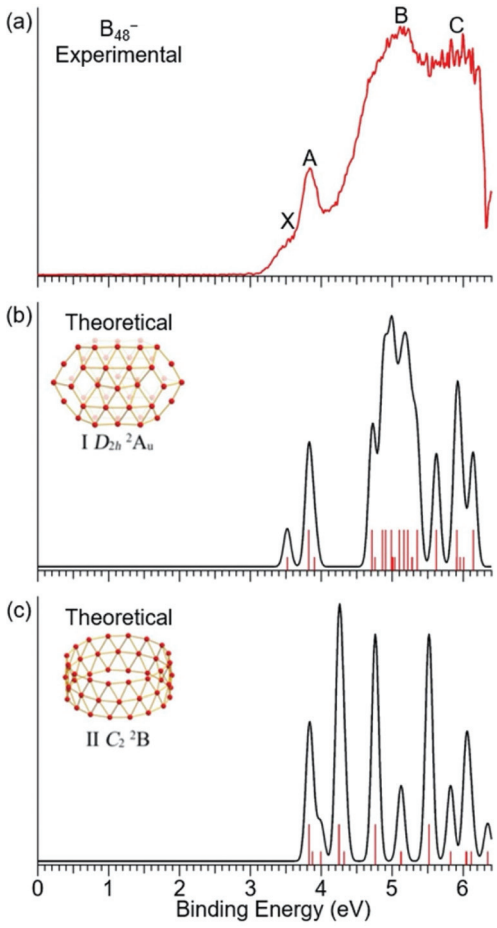

Fig. 3 Comparison of the simulated spectra of the bilayer B_{48}^- (I) (b) and the tubular B_{48}^- (II) (c) with the 193 nm spectrum (a). The theoretical VDEs were calculated at the TD-DFT/PBE0/6-311+G(d) level and plotted as vertical bars in (b) and (c). The longer bars are for the triplet final states and the shorter bars for the singlet final states. The simulated spectra were obtained by fitting the calculated VDEs with unit-area Gaussians of 0.1 eV width.

It can be seen that the simulated spectral pattern of the bilayer global minimum D_{2h} B_{48}^- (**I**) agrees well with the experimental spectrum. The D_{2h} B_{48}^- has a doublet ground state (^2A_u) with one unpaired electron in its highest occupied molecular orbital (HOMO, $6a_u$) (Table 1). Thus, both singlet and triplet final states are possible upon one electron detachment. Detaching one electron from the singly occupied HOMO ($6a_u$) of B_{48}^- (**I**) leads to the singlet ground state of neutral D_{2h} B_{48} (^1A_g) with a calculated VDE of 3.52 eV, in excellent agreement with the experimental VDE of 3.56 eV (Table 1). The calculated ADE of 3.41 eV compares well with the estimated experimental ADE of 3.3 eV, which carries a large uncertainty because of the tail on the low binding energy side of the X band due to hot band transitions (Fig. 1). Removal of one electron from the HOMO−1 ($14a_g$) results in a triplet (^3A_u) and a singlet (^1A_u) final state with the computed VDEs of 3.82 eV and 3.90 eV, respectively, in excellent agreement with band A at 3.87 eV. Following an energy gap of 0.81 eV, the next fourteen calculated VDEs originating from detaching one electron from the inner shells of the D_{2h} B_{48}^- (**I**) fall in the energy range between 4.71–5.35 eV, consistent with the broad spectral feature designated by B. The computed VDEs for the next six detachment channels are in the energy range of 5.62–6.14 eV and should correspond to the broad spectral feature designated by C. Overall, the simulated spectrum of the D_{2h} B_{48}^- (**I**) is in excellent agreement with the experimental data, lending considerable credence to the identified bilayer global minimum for B_{48}^-.

The calculated VDEs for the lowest-lying triple-ring tubular C_2 B_{48}^- (**II**) (^2B) isomer are higher than the experimental data (Fig. 3c). The simulated spectral pattern of this isomer is relatively simple in the higher binding energy side, also inconsistent with the experimental data at 193 nm. Furthermore, the tubular isomer is significantly higher in energy than the bilayer global minimum and it can be ruled out as a discernible contributor to the PE spectra of B_{48}^-.

5. Discussion

5.1 Bonding analyses

To understand the structure and stability of the bilayer global minimum for $B_{48}^{-/0}$, we performed ELF and AdNDP bonding analyses on the closed-shell D_{2h} B_{48} (**VII**), as shown in Fig. 4. The ELF_σ result (Fig. 4a) indicates the existence of localized B–B σ-bonds both on the periphery and between the top and bottom layers and delocalized in-plane σ bonds among the inner boron atoms, while the ELF_π pattern shows the formation of two local π-systems on both the top and bottom layers. The bonding picture provided by the ELF is consistent with the AdNDP bonding analyses, as shown in Fig. 4b. The first row of Fig. 4b presents 58 σ bonds for the bilayer B_{48}, including two 2c–2e interlayer B–B σ-bonds, sixteen 2c–2e B–B σ-bonds on the periphery, sixteen 3c–2e σ-bonds bridging the in-plane and peripheral atoms, four 3c–2e σ-bonds on the periphery bridging the top and bottom layers, and twelve 3c–2e

Table 1 Comparison between the experimentally measured vertical detachment energies and calculated VDEs of D_{2h} B_{48}^- (I) at TD-PBE0/6-311+G (d) level in eV

Band	VDE (expt.)	Final states and electron configurations	VDE (theo.)
X[a]	3.56[b]	^1A_g {...$6b_{2g}^2 12a_g^2 8b_{1g}^2 10b_{3u}^2 7b_{2g}^2 7b_{3g}^2 5a_u^2 10b_{2u}^2 11b_{3u}^2 13a_g^2 11b_{2u}^2 9b_{1u}^2 14a_g^2$ **$6a_u^0$**}	3.52
A	3.87[b]	^3A_u {...$6b_{2g}^2 12a_g^2 8b_{1g}^2 10b_{3u}^2 7b_{2g}^2 7b_{3g}^2 5a_u^2 10b_{2u}^2 11b_{3u}^2 13a_g^2 11b_{2u}^2 9b_{1u}^2$ **$14a_g^1$** $6a_u^1$}	3.82
		^1A_u {...$6b_{2g}^2 12a_g^2 8b_{1g}^2 10b_{3u}^2 7b_{2g}^2 7b_{3g}^2 5a_u^2 10b_{2u}^2 11b_{3u}^2 13a_g^2 11b_{2u}^2 9b_{1u}^2$ **$14a_g^1$** $6a_u^1$}	3.90
B	~5.1	$^3B_{1g}$ {...$6b_{2g}^2 12a_g^2 8b_{1g}^2 10b_{3u}^2 7b_{2g}^2 7b_{3g}^2 5a_u^2 10b_{2u}^2 11b_{3u}^2 13a_g^2 11b_{2u}^2$ **$9b_{1u}^1$** $14a_g^2 6a_u^1$}	4.71
		$^1B_{1g}$ {...$6b_{2g}^2 12a_g^2 8b_{1g}^2 10b_{3u}^2 7b_{2g}^2 7b_{3g}^2 5a_u^2 10b_{2u}^2 11b_{3u}^2 13a_g^2 11b_{2u}^2$ **$9b_{1u}^1$** $14a_g^2 6a_u^1$}	4.75
		$^3B_{2g}$ {...$6b_{2g}^2 12a_g^2 8b_{1g}^2 10b_{3u}^2 7b_{2g}^2 7b_{3g}^2 5a_u^2 10b_{2u}^2 11b_{3u}^2 13a_g^2$ **$11b_{2u}^1$** $9b_{1u}^2 14a_g^2 6a_u^1$}	4.86
		^3A_u {...$6b_{2g}^2 12a_g^2 8b_{1g}^2 10b_{3u}^2 7b_{2g}^2 7b_{3g}^2 5a_u^2 10b_{2u}^2$ **$11b_{3u}^1$** $13a_g^2 11b_{2u}^2 9b_{1u}^2 14a_g^2 6a_u^1$}	4.91
		$^3B_{3g}$ {...$6b_{2g}^2 12a_g^2 8b_{1g}^2 10b_{3u}^2 7b_{2g}^2 7b_{3g}^2 5a_u^2 10b_{2u}^2 11b_{3u}^2$ **$13a_g^1$** $11b_{2u}^2 9b_{1u}^2 14a_g^2 6a_u^1$}	4.99
		^1A_u {...$6b_{2g}^2 12a_g^2 8b_{1g}^2 10b_{3u}^2 7b_{2g}^2 7b_{3g}^2 5a_u^2 10b_{2u}^2$ **$11b_{3u}^1$** $13a_g^2 11b_{2u}^2 9b_{1u}^2 14a_g^2 6a_u^1$}	5.00
		$^1B_{2g}$ {...$6b_{2g}^2 12a_g^2 8b_{1g}^2 10b_{3u}^2 7b_{2g}^2 7b_{3g}^2 5a_u^2 10b_{2u}^2 11b_{3u}^2 13a_g^2$ **$11b_{2u}^1$** $9b_{1u}^2 14a_g^2 6a_u^1$}	5.01
		$^1B_{3g}$ {...$6b_{2g}^2 12a_g^2 8b_{1g}^2 10b_{3u}^2 7b_{2g}^2 7b_{3g}^2 5a_u^2 10b_{2u}^2 11b_{3u}^2$ **$13a_g^1$** $11b_{2u}^2 9b_{1u}^2 14a_g^2 6a_u^1$}	5.04
		$^3B_{2g}$ {...$6b_{2g}^2 12a_g^2 8b_{1g}^2 10b_{3u}^2 7b_{2g}^2 7b_{3g}^2 5a_u^2$ **$10b_{2u}^1$** $11b_{3u}^2 13a_g^2 11b_{2u}^2 9b_{1u}^2 14a_g^2 6a_u^1$}	5.10
		^3A_g {...$6b_{2g}^2 12a_g^2 8b_{1g}^2 10b_{3u}^2 7b_{2g}^2 7b_{3g}^2$ **$5a_u^1$** $10b_{2u}^2 11b_{3u}^2 13a_g^2 11b_{2u}^2 9b_{1u}^2 14a_g^2 6a_u^1$}	5.17
		$^3B_{3u}$ {...$6b_{2g}^2 12a_g^2 8b_{1g}^2 10b_{3u}^2 7b_{2g}^2$ **$7b_{3g}^1$** $5a_u^2 10b_{2u}^2 11b_{3u}^2 13a_g^2 11b_{2u}^2 9b_{1u}^2 14a_g^2 6a_u^1$}	5.22
		^1A_g {...$6b_{2g}^2 12a_g^2 8b_{1g}^2 10b_{3u}^2 7b_{2g}^2 7b_{3g}^2$ **$5a_u^1$** $10b_{2u}^2 11b_{3u}^2 13a_g^2 11b_{2u}^2 9b_{1u}^2 14a_g^2 6a_u^1$}	5.28
		$^1B_{2g}$ {...$6b_{2g}^2 12a_g^2 8b_{1g}^2 10b_{3u}^2 7b_{2g}^2 7b_{3g}^2 5a_u^2$ **$10b_{2u}^1$** $11b_{3u}^2 13a_g^2 11b_{2u}^2 9b_{1u}^2 14a_g^2 6a_u^1$}	5.28
		$^3B_{2u}$ {...$6b_{2g}^2 12a_g^2 8b_{1g}^2 10b_{3u}^2$ **$7b_{2g}^1$** $7b_{3g}^2 5a_u^2 10b_{2u}^2 11b_{3u}^2 13a_g^2 11b_{2u}^2 9b_{1u}^2 14a_g^2 6a_u^1$}	5.35
C	~5.9	$^3B_{3g}$ {...$6b_{2g}^2 12a_g^2 8b_{1g}^2$ **$10b_{3u}^1$** $7b_{2g}^2 7b_{3g}^2 5a_u^2 10b_{2u}^2 11b_{3u}^2 13a_g^2 11b_{2u}^2 9b_{1u}^2 14a_g^2 6a_u^1$}	5.62
		$^1B_{3u}$ {...$6b_{2g}^2 12a_g^2 8b_{1g}^2 10b_{3u}^2 7b_{2g}^2$ **$7b_{3g}^1$** $5a_u^2 10b_{2u}^2 11b_{3u}^2 13a_g^2 11b_{2u}^2 9b_{1u}^2 14a_g^2 6a_u^1$}	5.91
		$^3B_{1u}$ {...$6b_{2g}^2 12a_g^2$ **$8b_{1g}^1$** $10b_{3u}^2 7b_{2g}^2 7b_{3g}^2 5a_u^2 10b_{2u}^2 11b_{3u}^2 13a_g^2 11b_{2u}^2 9b_{1u}^2 14a_g^2 6a_u^1$}	5.91
		$^1B_{2u}$ {...$6b_{2g}^2 12a_g^2 8b_{1g}^2 10b_{3u}^2$ **$7b_{2g}^1$** $7b_{3g}^2 5a_u^2 10b_{2u}^2 11b_{3u}^2 13a_g^2 11b_{2u}^2 9b_{1u}^2 14a_g^2 6a_u^1$}	5.96
		$^1B_{3g}$ {...$6b_{2g}^2 12a_g^2 8b_{1g}^2$ **$10b_{3u}^1$** $7b_{2g}^2 7b_{3g}^2 5a_u^2 10b_{2u}^2 11b_{3u}^2 13a_g^2 11b_{2u}^2 9b_{1u}^2 14a_g^2 6a_u^1$}	6.01
		$^3B_{1u}$ {...$6b_{2g}^2 12a_g^2$ **$8b_{1g}^1$** $10b_{3u}^2 7b_{2g}^2 7b_{3g}^2 5a_u^2 10b_{2u}^2 11b_{3u}^2 13a_g^2 11b_{2u}^2 9b_{1u}^2 14a_g^2 6a_u^1$}	6.14

[a] The ADE or the EA of B_{48} was estimated to be 3.3 ± 0.1 eV. [b] The uncertainty was ±0.02 eV.

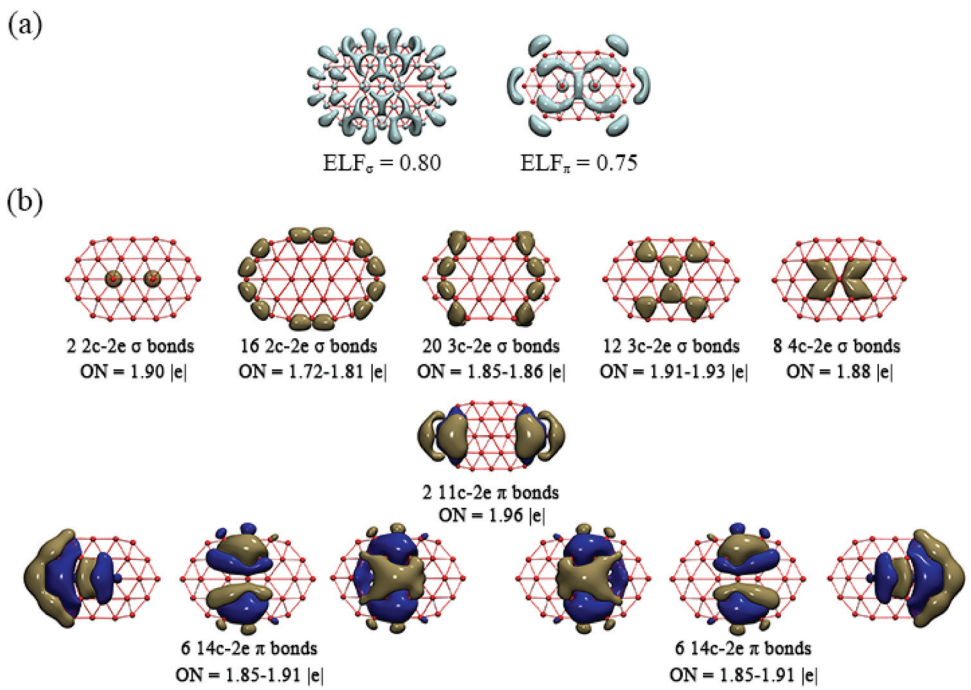

Fig. 4 Chemical bonding analyses for the global minimum bilayer structure of B_{48} (D_{2h}). (a) The ELF analysis. (b) The AdNDP bonding patterns. ON stands for occupation numbers.

and eight 4c–2e in-plane σ-bonds on the top and bottom layers. The remaining 14 pairs of electrons form the π-bonding system over the bilayer surface, including two 11c–2e π-bonds on the waist at the two ends in the second row of Fig. 4b and twelve 14c–2e π bonds symmetrically distributed on the top and bottom B_{19} layers in the third row. The twelve delocalized

14c–2e π bonds can be viewed as four 14c–2e π systems, forming two equivalent 6π aromatic systems on each of the top and bottom layers. The corresponding π CMOs are presented in Fig. S3,† which display similarities to the AdNDP results, but the AdNDP analyses provide a more succinct bonding picture. Such a bonding pattern renders 3D aromaticity to the D_{2h} B_{48} (**VII**) cluster, as evidenced by the negative value of the nucleus independent chemical shift (−25.87 ppm at its geometrical center).[61]

5.2 On the stability of the bilayer B_{48} cluster

To provide further insight into the stability of the bilayer structure of B_{48}, we calculated its cohesive energy per atom (E_{coh}) at the PBE0 level, as compared with other known smaller boron clusters (Fig. 5). The E_{coh} generally increases with the cluster size from B_7 to B_{48}. Overall, 2D structures dominate in this size range. Even though tubular structures appear at B_{20}, only 2D structures were observed for the B_{20}^- anion.[9,62] Low-lying cage-like borospherene structures start to emerge at B_{28}.[29,30] The D_{2d} B_{40} borospherene is known to be overwhelmingly more stable than its 2D counterparts.[27] The bilayer B_{48} turns out to be more stable than the 2D isomer (**XI**) by 0.031 eV per atom and more stable than the cage isomer (**XII**) by 0.033 eV per atom, most likely due to the additional interlayer covalent bonding. Clearly, the electron deficiency of boron makes its bonding much more promiscuous that carbon. We have also done BOMD simulations, which indicate that both the bilayer B_{48}^- and B_{48} clusters are dynamically stable even at 1000 K with small average root-mean-square-deviations (RMSD) of 0.18, 0.17 Å and maximum bond length deviations (MAXD) of 0.80, 0.77 Å, respectively (Fig. S4†).

5.3 Towards the formation of 2D bilayer borophenes

Bilayer borophenes with various structures and interesting properties have been proposed computationally.[63–69] The observation of the bilayer B_{48}^- cluster in the gas phase provides experimental evidence about the viability of bilayer borophenes. Using the bilayer B_{48} cluster as a structural motif, one can construct different bilayer borophenes. Sai *et al.* considered the eclipsed B_{30} bilayer borophene in A–A packing (Fig. 6a).[34] We have constructed the staggered B_{30} bilayer borophene in A–B packing, as shown in Fig. 6b with the hole distribution pattern rotated by 60° in the bottom layer. The two structures are found to have similar cohesive energies with E_{coh} = 6.204 eV per atom and 6.178 eV per atom at the PBE level, respectively. Both the eclipsed and staggered bilayer borophenes contain four interlayer B–B σ-bonds involving eight inward-buckled atoms in each unit cell, with an inward-buckled atom density of η_{inward} = 4/15 and a hole density of η_{hole} = 1/16. We also considered several other bilayer borophenes, as shown in Fig. S5.† We found that the two most stable bilayer borophenes are 0.149 and 0.122 eV per atom more stable than the previously reported prototypical monolayer boron α-sheet ($\eta_{1/9}$),[70] respectively, where the energy

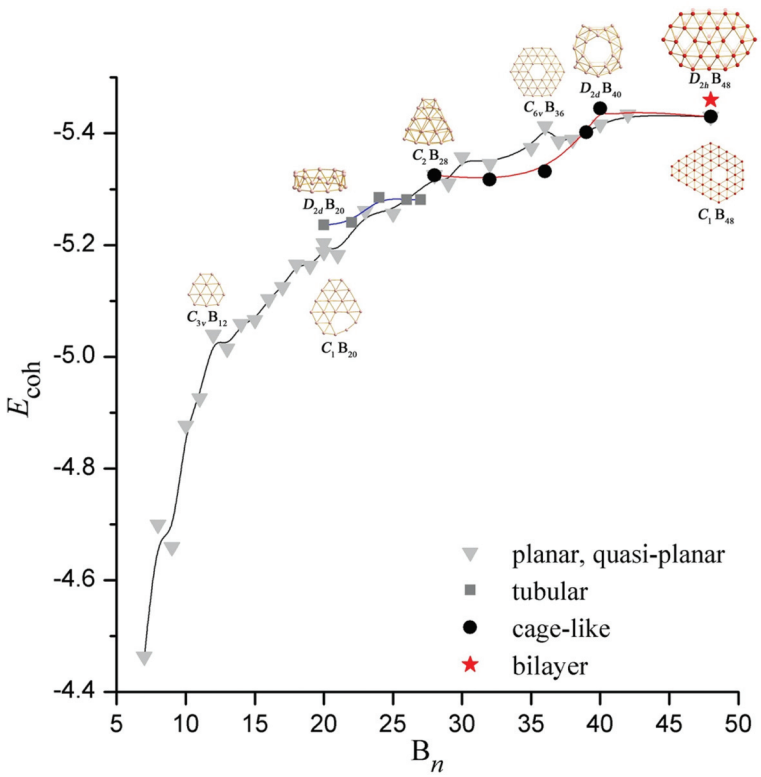

Fig. 5 The calculated cohesive energies per atom (E_{coh}) for the neutral B_n (n = 7–48) clusters at the PBE0/6-311+G(d) level of theory. The lines are drawn to guide the eyes.

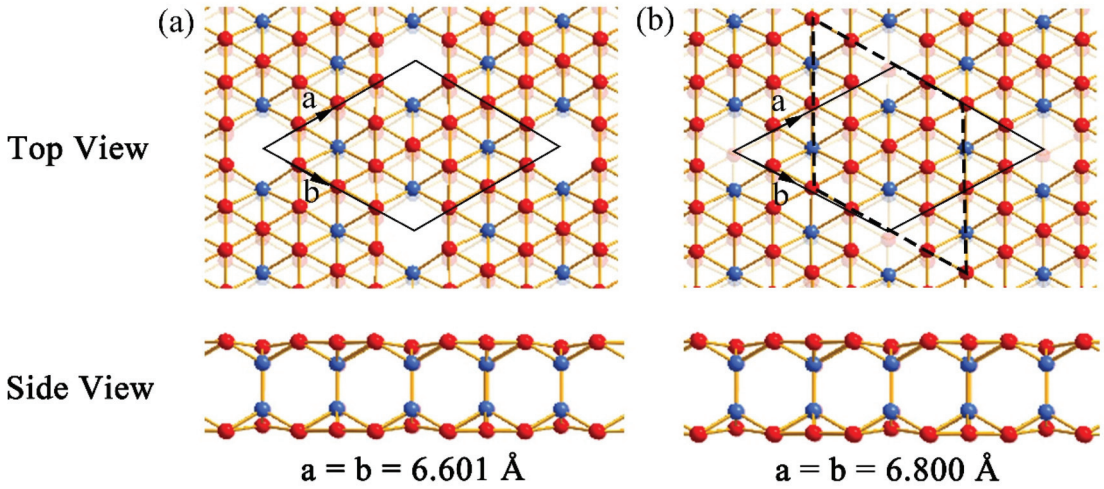

Fig. 6 Top and side views of (a) the eclipsed B_{30} bilayer borophene (A–A packing)[34] and (b) staggered B_{30} bilayer borophene (A–B packing) based on the structural motif of the D_{2h} B_{48}, with the optimized lattice parameters (*a* and *b*) given at the PBE level. The inward-buckled atoms forming the interlayer B–B σ-bonds are highlighted in blue.

differences between the most stable monolayer borophenes are less than 10 meV per atom at different theoretical levels.[71–73] Monolayer borophenes have been synthesized on metal substrates.[20,21] However, no free-standing monolayer borophenes have been realized to date. With their higher stability, free-standing bilayer borophenes may be viable and should be promising targets for future experimental syntheses.

6. Conclusions

We report a joint photoelectron spectroscopy and theoretical investigation of the structures, bonding and stability of the $B_{48}^{-/0}$ clusters. Characteristic photoelectron spectral features were observed for B_{48}^- and used to verify its global minimum, which was found to have a D_{2h} bilayer structure similar to the B_{48} neutral. At our highest level of theory, we found that the bilayer structures of $B_{48}^{-/0}$ are much more stable than other isomers. The bilayer structures feature interlayer σ and π bonding interactions, underlying its relatively high stability. The current work further demonstrates the structural diversity of boron nanoclusters and provides experimental evidence for the viability of bilayer borophenes.

Conflicts of interest

There are no conflicts to declare.

Acknowledgements

The experimental work done at Brown University was supported by the U.S. National Science Foundation (CHE-1763380). The theoretical work was supported by the National Natural Science Foundation of China (No. 21720102006, 21973057, and 22003034).

References

1 B. Albert and H. Hillebrecht, *Angew. Chem., Int. Ed.*, 2009, **48**, 8640–8668.
2 A. R. Oganov, J. Chen, C. Gatti, Y. Ma, Y. Ma, C. W. Glass, Z. Liu, T. Yu, O. O. Kurakevych and V. L. Solozhenko, *Nature*, 2009, **457**, 863–867.
3 W. N. Lipscomb, *Science*, 1977, **196**, 1047–1055.
4 H. J. Zhai, L. S. Wang, A. N. Alexandrova and A. I. Boldyrev, *J. Chem. Phys.*, 2002, **117**, 7917–7924.
5 H. J. Zhai, B. Kiran, J. Li and L. S. Wang, *Nat. Mater.*, 2003, **2**, 827–833.
6 A. N. Alexandrova, A. I. Boldyrev, H. J. Zhai and L. S. Wang, *Coord. Chem. Rev.*, 2006, **250**, 2811–2866.
7 E. Oger, N. R. M. Crawford, R. Kelting, P. Weis, M. M. Kappes and R. Ahlrichs, *Angew. Chem., Int. Ed.*, 2007, **46**, 8503–8506.
8 W. Huang, A. P. Sergeeva, H. J. Zhai, B. B. Averkiev, L. S. Wang and A. I. Boldyrev, *Nat. Chem.*, 2010, **2**, 202–206.
9 L. S. Wang, *Int. Rev. Phys. Chem.*, 2016, **35**, 69–142.
10 M. R. Fagiani, X. W. Song, P. Petrov, S. Debnath, S. Gewinner, W. Schollkopf, T. Heine, A. Fielicke and K. R. Asmis, *Angew. Chem., Int. Ed.*, 2017, **56**, 501–504.
11 W. L. Li, X. Chen, T. Jian, T. T. Chen, J. Li and L. S. Wang, *Nat. Rev. Chem.*, 2017, **1**, 0071.
12 W. L. Li, H. S. Hu, Y. F. Zhao, X. Chen, T. T. Chen, T. Jian, L. S. Wang and J. Li, *Sci. Sin.: Chim.*, 2018, **48**, 98–107.
13 T. Jian, X. Chen, S. D. Li, A. I. Boldyrev, J. Li and L. S. Wang, *Chem. Soc. Rev.*, 2019, **48**, 3550–3591.
14 S. Pan, J. Barroso, S. Jalife, T. Heine, K. R. Asmis and G. Merino, *Acc. Chem. Res.*, 2019, **52**, 2732–2744.

15 A. P. Sergeeva, I. A. Popov, Z. A. Piazza, W. L. Li, C. Romanescu, L. S. Wang and A. I. Boldyrev, *Acc. Chem. Res.*, 2014, **47**, 1349–1358.
16 A. I. Boldyrev and L. S. Wang, *Phys. Chem. Chem. Phys.*, 2016, **18**, 11589–11605.
17 Z. A. Piazza, H. S. Hu, W. L. Li, Y. F. Zhao, J. Li and L. S. Wang, *Nat. Commun.*, 2014, **5**, 3113.
18 Q. Chen, G. F. Wei, W. J. Tian, H. Bai, Z. P. Liu, H. J. Zhai and S. D. Li, *Phys. Chem. Chem. Phys.*, 2014, **16**, 18282–18287.
19 W. L. Li, Q. Chen, W. J. Tian, H. Bai, Y. F. Zhao, H. S. Hu, J. Li, H. J. Zhai, S. D. Li and L. S. Wang, *J. Am. Chem. Soc.*, 2014, **136**, 12257–12260.
20 A. J. Mannix, X. F. Zhou, B. Kiraly, J. D. Wood, D. Alducin, B. D. Myers, X. L. Liu, B. L. Fisher, U. Santiago, J. R. Guest, M. J. Yacaman, A. Ponce, A. R. Oganov, M. C. Hersam and N. P. Guisinger, *Science*, 2015, **350**, 1513–1516.
21 B. Feng, J. Zhang, Q. Zhong, W. Li, S. Li, H. Li, P. Cheng, S. Meng, L. Chen and K. Wu, *Nat. Chem.*, 2016, **8**, 563–568.
22 Z. Zhang, E. S. Penev and B. I. Yakobson, *Chem. Soc. Rev.*, 2017, **46**, 6746–6763.
23 L. Kong, K. Wu and L. Chen, *Front. Phys.*, 2018, **13**, 138105.
24 A. J. Mannix, Z. Zhang, N. P. Guisinger, B. I. Yakobson and M. C. Hersam, *Nat. Nanotechnol.*, 2018, **13**, 444–450.
25 S. Y. Xie, Y. Wang and X. B. Li, *Adv. Mater.*, 2019, **31**, 1900392.
26 H. Bai, T. T. Chen, Q. Chen, X. Y. Zhao, Y. Y. Zhang, W. J. Chen, W. L. Li, L. F. Cheung, B. Bai, J. Cavanagh, W. Huang, S. D. Li, J. Li and L. S. Wang, *Nanoscale*, 2019, **11**, 23286–23295.
27 H. J. Zhai, Y. F. Zhao, W. L. Li, Q. Chen, H. Bai, H. S. Hu, Z. A. Piazza, W. J. Tian, H. G. Lu, Y. B. Wu, Y. W. Mu, G. F. Wei, Z. P. Liu, J. Li, S. D. Li and L. S. Wang, *Nat. Chem.*, 2014, **6**, 727–731.
28 Q. Chen, W. L. Li, Y. F. Zhao, S. Y. Zhang, H. S. Hu, H. Bai, H. R. Li, W. J. Tian, H. G. Lu, H. J. Zhai, S. D. Li, J. Li and L. S. Wang, *ACS Nano*, 2015, **9**, 754–760.
29 J. Zhao, X. Huang, R. Shi, H. Liu, Y. Su and R. B. King, *Nanoscale*, 2015, **7**, 15086–15090.
30 Y. J. Wang, Y. F. Zhao, W. L. Li, T. Jian, Q. Chen, X. R. You, T. Ou, X. Y. Zhao, H. J. Zhai, S. D. Li, J. Li and L. S. Wang, *J. Chem. Phys.*, 2016, **144**, 064307.
31 H. R. Li, T. Jian, W. L. Li, C. Q. Miao, Y. J. Wang, Q. Chen, X. M. Luo, K. Wang, H. J. Zhai, S. D. Li and L. S. Wang, *Phys. Chem. Chem. Phys.*, 2016, **18**, 29147–29155.
32 S. G. Xu, Y. J. Zhao, J. H. Liao and X. B. Yang, *J. Chem. Phys.*, 2015, **142**, 214307.
33 S. G. Xu, Y. J. Zhao, X. B. Yang and H. Xu, *J. Phys. Chem. C*, 2017, **121**, 11950–11955.
34 L. Sai, X. Wu, N. Gao, J. Zhao and R. B. King, *Nanoscale*, 2017, **9**, 13905–13909.
35 L. Pei, Y. Y. Ma, M. Yan, M. Zhang, R. N. Yuan, Q. Chen, W. Y. Zan, Y. W. Mu and S. D. Li, *Eur. J. Inorg. Chem.*, 2020, 3296–3301.
36 L. S. Wang, H. S. Cheng and J. Fan, *J. Chem. Phys.*, 1995, **102**, 9480–9493.
37 Y. Zhao, X. Chen and J. Li, *Nano Res.*, 2017, **10**, 3407–3420.
38 X. Chen, Y.-F. Zhao, L. S. Wang and J. Li, *Comput. Theor. Chem.*, 2017, **1107**, 57–65.
39 X. Chen, Y. F. Zhao, Y. Y. Zhang and J. Li, *J. Comput. Chem.*, 2019, **40**, 1105–1112.
40 C. Adamo and V. Barone, *J. Chem. Phys.*, 1999, **110**, 6158–6170.
41 V. N. Staroverov, G. E. Scuseria, J. M. Tao and J. P. Perdew, *J. Chem. Phys.*, 2003, **119**, 12129–12137.
42 R. Krishnan, J. S. Binkley, R. Seeger and J. A. Pople, *J. Chem. Phys.*, 1980, **72**, 650–654.
43 J. Čížek, *Adv. Chem. Phys.*, 1969, **14**, 35–88.
44 G. D. Purvis and R. J. Bartlett, *J. Chem. Phys.*, 1982, **76**, 1910–1918.
45 K. Raghavachari, G. W. Trucks, J. A. Pople and M. Head-Gordon, *Chem. Phys. Lett.*, 1989, **157**, 479–483.
46 R. Bauernschmitt and R. Ahlrichs, *Chem. Phys. Lett.*, 1996, **256**, 454–464.
47 M. E. Casida, C. Jamorski, K. C. Casida and D. R. Salahub, *J. Chem. Phys.*, 1998, **108**, 4439–4449.
48 M. J. Frisch, G. W. Trucks, H. B. Schlegel, G. E. Scuseria, M. A. Robb, J. R. Cheeseman, *et al.*, *Gaussian 09, Revision D.01*, Gaussian, Inc., Wallingford, CT, 2009.
49 H. J. Werner, P. J. Knowles, G. Knizia, F. R. Manby, M. Schütz, P. Celani, *et al.*, *MOLPRO, version 2012.1*.
50 B. Silvi and A. Savin, *Nature*, 1994, **371**, 683–686.
51 D. Y. Zubarev and A. I. Boldyrev, *Phys. Chem. Chem. Phys.*, 2008, **10**, 5207–5217.
52 N. V. Tkachenko and A. I. Boldyrev, *Phys. Chem. Chem. Phys.*, 2019, **21**, 9590–9596.
53 W. Humphrey, A. Dalke and K. Schulten, *J. Mol. Graphics*, 1996, **14**, 33–38.
54 J. V. Vondele, M. Krack, F. Mohamed, M. Parrinello, T. Chassaing and J. Hutter, *Comput. Phys. Commun.*, 2005, **167**, 103–128.
55 J. P. Perdew, K. Burke and M. Ernzerhof, *Phys. Rev. Lett.*, 1996, **77**, 3865–3868.
56 P. E. Blöchl, *Phys. Rev. B: Condens. Matter Mater. Phys.*, 1994, **50**, 17953–17979.
57 G. Kresse and D. Joubert, *Phys. Rev. B: Condens. Matter Mater. Phys.*, 1999, **59**, 1758–1775.
58 G. Kresse and J. Furthmüller, *Comput. Mater. Sci.*, 1996, **6**, 15–50.
59 G. Kresse and J. Furthmüller, *Phys. Rev. B: Condens. Matter Mater. Phys.*, 1996, **54**, 11169–11186.
60 X. Wu, L. Sai, S. Zhou, P. Zhou, M. Chen, M. Springborg and J. Zhao, *Phys. Chem. Chem. Phys.*, 2020, **22**, 12959–12966.
61 P. v. R. Schleyer, C. Maerker, A. Dransfeld, H. Jiao and N. J. v. E. Hommes, *J. Am. Chem. Soc.*, 1996, **118**, 6317–6318.
62 B. Kiran, S. Bulusu, H. J. Zhai, S. Yoo, X. C. Zeng and L. S. Wang, *Proc. Natl. Acad. Sci. U. S. A.*, 2005, **102**, 961–964.
63 X. F. Zhou, X. Dong, A. R. Oganov, Q. Zhu, Y. Tian and H. T. Wang, *Phys. Rev. Lett.*, 2014, **112**, 085502.

64 F. Ma, Y. Jiao, G. Gao, Y. Gu, A. Bilic, Z. Chen and A. Du, *Nano Lett.*, 2016, **16**, 3022–3028.
65 Y. Zhao, S. Zeng and J. Ni, *Phys. Rev. B*, 2016, **93**, 014502.
66 N. Karmodak and E. D. Jemmis, *J. Phys. Chem. C*, 2018, **122**, 2268–2274.
67 N. Gao, X. Wu, X. Jiang, Y. Bai and J. Zhao, *FlatChem*, 2018, **7**, 48–54.
68 H. Zhong, K. Huang, G. Yu and S. Yuan, *Phys. Rev. B*, 2018, **98**, 054104.
69 S. G. Xu, B. Zheng, H. Xu and X. B. Yang, *J. Phys. Chem. C*, 2019, **123**, 4977–4983.
70 H. Tang and S. Ismail-Beigi, *Phys. Rev. Lett.*, 2007, **99**, 115501.
71 X. Wu, J. Dai, Y. Zhao, Z. Zhuo, J. Yang and X. C. Zeng, *ACS Nano*, 2012, **6**, 7443–7453.
72 H. Lu, Y. Mu, H. Bai, Q. Chen and S. D. Li, *J. Chem. Phys.*, 2013, **138**, 024701.
73 S. G. Xu, X. T. Li, Y. J. Zhao, J. H. Liao, H. Xu and X. B. Yang, *Nanoscale*, 2018, **10**, 13410–13416.